

Wavefront sensing and reconstruction from gradient and Laplacian data measured with a Hartmann–Shack sensor

Sergio Barbero

School of Optometry, Indiana University, Bloomington, Indiana 47405

Jacob Rubinstein

Department of Mathematics, Indiana University, Bloomington, Indiana 47405

Larry N. Thibos

School of Optometry, Indiana University, Bloomington, Indiana 47405

Received January 13, 2006; revised March 29, 2006; accepted March 30, 2006; posted March 31, 2006 (Doc. ID 67238)

A new wavefront sensing and reconstruction technique is presented. It is possible to measure Laplacian and gradient information of a wavefront with a Hartmann–Shack setup. By simultaneously using the Laplacian and gradient data we reconstruct the wavefront by sequentially solving two partial differential equations.

© 2006 Optical Society of America
OCIS codes: 010.7350, 080.2720.

Wavefront sensing and reconstruction is a broad area in optics with many applications, including adaptive optics technology,¹ phase imaging,² and visual optics.³ Wavefront sensing is the physical technique used to obtain information on the wavefront, typically in the form of gradient data [Hartmann–Shack (H–S) sensors, shear interferometry, etc.] or curvature (Laplacian) data (e.g., curvature sensors). Wavefront reconstruction is the mathematical technique used to reconstruct the wavefront surface from the data collected in wavefront sensing. In this Letter we present two novel ideas, one in the field of wavefront sensing and the other in wavefront reconstruction. We propose a wavefront sensor that measures gradient and Laplacian data simultaneously with a single experimental setup (H–S). In addition, we derive the necessary mathematical formulation to reconstruct the wavefront surface from both data types simultaneously, rather than using gradient or Laplacian data independently.

There is a common basis that relates gradient and curvature wavefront sensors. The phase and the intensity of a wave propagating in a homogeneous medium are related by a partial differential equation (PDE) derived by Sommerfeld and Runge in 1911.⁴ Gradient and curvature sensors assume that the wavefront obeys the paraxial approximation of this equation, the so-called transport-of-intensity equation (TIE). This way, TIE is the basic tool in curvature sensing following the suggestion of Teague⁵ and others. The link between TIE and gradient sensors (specifically H–S sensors) has been shown by Bara.⁶ This common theoretical framework for Laplacian and gradient measurements suggests the possibility of using a H–S sensor to measure not only gradient data but also Laplacian data.

Figure 1 shows the procedure used to measure combined gradient and Laplacian data. Two H–S images of an incoming wavefront are captured at two axial locations. This can be done, experimentally, in different ways: moving the H–S sensor axially, using a beam splitter, etc. The intensity difference between corresponding spots in the two images is used to approximate the partial derivative of the intensity with respect to the z axis (optical axis). In most practical applications it is reasonable to assume that the spatial intensity distribution is nearly constant over the surface of a microlens in the H–S array. This assumption is used to simplify the paraxial TIE to

$$\Delta u = -(\partial I / \partial z) / I. \quad (1)$$

Here u and I are the phase and intensity, respectively, and the Laplacian operator (Δ) is considered over a plane perpendicular to the axis of propagation. The left-hand side of Eq. (1) quantifies the curvature of the wavefront, and the right-hand side is the ratio between the derivative of the intensity with respect to z (evaluated as spot energy difference) and the total intensity (computed as the energy of each spot). Such a procedure is expected to be robust with respect to the important problem of photodetection noise in curvature sensing,⁷ because the intensity is integrated over the pixels covering each spot. In a recent paper Paterson *et al.*⁸ suggested that a H–S sensor with cylindrical lenses be used to measure Laplacian data, although they did not propose an algorithm for reconstructing the wavefront from such data.

In practice, the experimentally measured gradient and Laplacian data will be affected by noise. Therefore one should seek an optimal estimate of the wave-

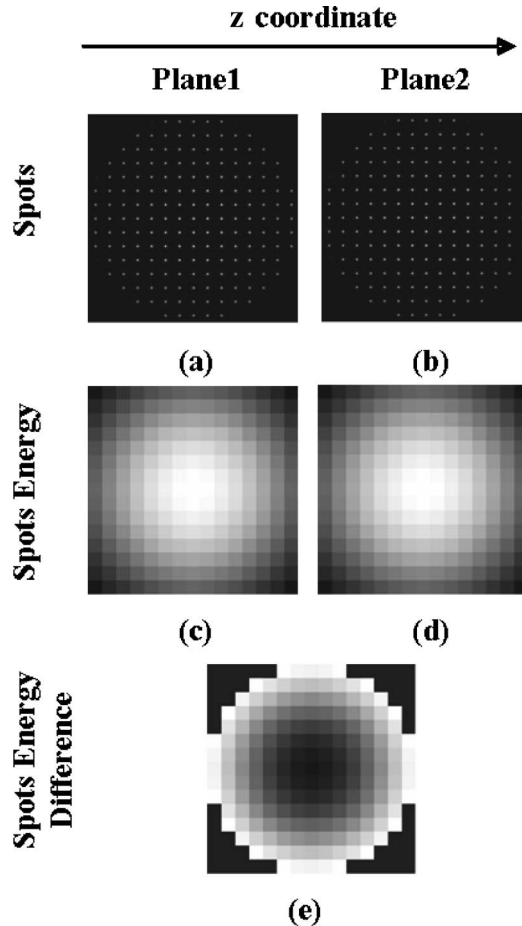


Fig. 1. (a), (b) Two H-S images are taken in two axial locations in the optical axis. The energy contained in each spot of the H-S images is computed to generate (c), (d) two spot energy maps. The difference between energy maps (d) and (c) is (e) the energy map necessary to compute Eq. (1).

front. For this purpose we estimate the phase function u by minimizing the least-squares functional:

$$\min K(u) \equiv \min \int \int_D (w|\nabla u - \vec{f}|^2 + |\Delta u - g|^2) dx dy. \quad (2)$$

Here \vec{f} and g are the experimentally measured gradient and Laplacian of u , respectively, and D is the domain where u is defined. Finally, w is a weight that balances the relative importance of the gradient and Laplacian data. For simplicity it is assumed here that w is constant. The variational problem expressed in Eq. (2) can be solved by computing the associated Euler-Lagrange equation⁹:

$$w(\nabla \cdot \vec{f} - \Delta u) + (\Delta^2 u - \Delta g) = 0. \quad (3)$$

Equation (3) is supplemented by two natural boundary conditions

$$w \partial_n u - \partial_n (\Delta u) = w \vec{f} \cdot \hat{n} - \partial_n g, \quad (4)$$

$$\Delta u = g,$$

where \hat{n} is the normal to the boundary of D and ∂_n denotes partial differentiation in the \hat{n} direction. Solving PDE (3), together with boundary conditions (4), provides the optimal phase estimate u . Differential equations of fourth order such as Eq. (3) are hard to solve numerically. Fortunately u appears in the equation only under the Laplacian operator Δ and the biharmonic operator Δ^2 . This feature, together with the special form of the boundary conditions, enables us to split the biharmonic problem into two second-order PDEs that are much easier to solve. Thus we define $v = \Delta u$ and write

$$\Delta v - wv = \Delta g - w \nabla \cdot \vec{f},$$

$$\text{boundary condition } v = g, \quad (5)$$

$$\Delta u = v,$$

$$\text{boundary condition } w \partial_n u = w \vec{f} \cdot \hat{n} - \partial_n g + \partial_n v. \quad (6)$$

Notice that Eq. (5) does not depend on u . Thus the single biharmonic equation was split into two second-order PDEs that can be solved sequentially.

In practice, the final PDEs in Eqs. (5) and (6) are solved by using numerical techniques, such as the finite difference method or the finite element method (FEM). We adopt a FEM solver mainly because for typical circular samplings of the wavefront the mesh generated in FEM is more adequate for points close to the edge than in the finite difference method.

Briefly, the FEM technique consists of discretizing the PDE; i.e., approximating the continuous solution by a discrete solution in a set of points defined by a mesh. The continuous problem is replaced by a system of linear equations defined with respect to the mesh. In the simulations performed for this Letter we used the mesh generator and linear algebra code available in Matlab Partial Differential Equation toolbox (version 7.0).

We simulated an asymmetric wavefront $u = 0.2Z_4^0 + 0.1Z_3^{-1}$. Here Z_m^n are Zernike polynomials,¹⁰ and the units are in micrometers. The wavefront is defined over a circular aperture of radius 3 mm, where we used 6000 points in the FEM mesh. Gaussian random noise was introduced in the gradient ($\sigma = 0.06$) and Laplacian data of the wavefront. It must be pointed out that in real H-S systems noise could be different from Gaussian because of the complexity of the error sources (e.g., lenslet size, spacing, diffraction effects, centroiding errors, etc.). We simulated three different amounts of noise in the Laplacian: noise level A ($\sigma = 0.07 \mu\text{m}^{-1}$), noise level B ($\sigma = 0.05 \mu\text{m}^{-1}$), and noise level C ($\sigma = 0.03 \mu\text{m}^{-1}$). Finally, we used five different values for the weight w (0.01, 0.1, 1, 10, 100) to study the relative contribution of gradient and Laplacian data in the accuracy of the reconstruction.

Figure 2 shows the results of this simulation. The optimal weight depends on the relative noise levels of the gradient and Laplacian data, which obviously depend on the specific setup and shape of the wavefront measured. It is observed that when the weight w is very small the solver is using mainly the Laplacian data, and the rms errors are ranked by the induced noise. As the weight w increases, the behavior in the three cases is not the same. For noise level A, the Laplacian data is too noisy, and one clearly benefits from increasing w , at least up to some value. On the other hand, the rms error for noise level C always increases with w , because the noise in the Laplacian data is less important than the noise in the gradient data. When w becomes too large, however, the rms errors increase for all three noise levels. We suspect that this happens because the large w is a singular limit for the differential equation (3).

We will provide a detailed description of the numerical method, together with extensive simulations and experimental data, in a forthcoming publication.

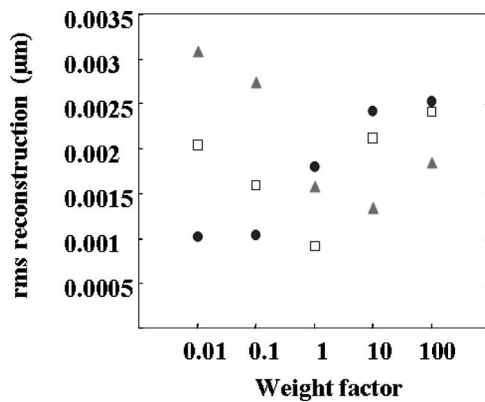


Fig. 2. Error in the wavefront reconstruction rms for different levels of simulated noise in the Laplacian data and values of the weight factor w . The FEM solver used 6000 mesh points. Symbols indicate different noise levels: triangles, level A; squares, level B; circles, level C.

Finally, it is worth noting that in the special situation of periodic wavefronts, inside the domain, it is possible to use a fast Fourier solver. Applying the discrete Fourier transform directly to PDE (3) and performing some analytical computations, the Fourier coefficients of the solution $[U(l, m)]$ are found to satisfy

$$U(l, m) = \frac{wk^2G(l^2 + m^2) - k(lF_x + mF_y)}{wk^4(l^2 + m^2)^2 - k^2(l^2 + m^2)}, \quad (7)$$

where G is the discrete Fourier coefficients of g (Laplacian data), F_x and F_y of f_x and f_y , respectively, and $k = 2\pi i$. The reconstructed wavefront is obtained from these Fourier coefficients by using the inverse Fourier transform.

S. Barbero's e-mail address is sbarber2@indiana.edu.

References

1. R. K. Tyson, *Principles of Adaptive Optics* (Academic, 1998).
2. K. A. Nugent, D. Paganin, and T. E. Gureyev, *Phys. Today* **54**, 27 (2001).
3. D. A. Atchison and G. Smith, *Optics of the Human Eye* (Butterworth-Heinemann, 2000).
4. A. Sommerfeld and J. I. Runge, *Ann. Phys.* **35**, 277 (1911).
5. M. R. Teague, *J. Opt. Soc. Am.* **73**, 1434 (1983).
6. S. Bara, *J. Opt. Soc. Am. A* **20**, 2237 (2003).
7. S. Barbero and L. N. Thibos, "Error analysis and correction in wavefront reconstruction from Transport-of-Intensity-Equation," *Opt. Eng.* (to be published).
8. C. Paterson and J. C. Dainty, *Opt. Lett.* **25**, 1687 (2000).
9. Y. Pinchover and J. Rubinstein, *Introduction to Partial Differential Equations* (Cambridge U. Press, 2005).
10. L. N. Thibos, R. A. Applegate, J. T. Schwiegerling, and R. Webb, *J. Refract. Surg.* **16**, S654 (2000).